Accepted Manuscript

Fibrosis rescue improves cardiac function in dystrophin-deficient mice and Duchenne patient–specific cardiomyocytes by immunoproteasome modulation

Andrea Farini, Aoife Gowran, Pamela Bella, Clementina Sitzia, Alessandro Scopece, Elisa Castiglioni, Davide Rovina, Patrizia Nigro, Chiara Villa, Francesco Fortunato, Giacomo Pietro Comi, Giuseppina Milano, Giulio Pompilio, Yvan Torrente

PII: S0002-9440(18)30370-5

DOI: https://doi.org/10.1016/j.ajpath.2018.10.010

Reference: AJPA 3031

To appear in: *The American Journal of Pathology*

Received Date: 23 April 2018

Revised Date: 12 September 2018

Accepted Date: 10 October 2018

Please cite this article as: Farini A, Gowran A, Bella P, Sitzia C, Scopece A, Castiglioni E, Rovina D, Nigro P, Villa C, Fortunato F, Comi GP, Milano G, Pompilio G, Torrente Y, Fibrosis rescue improves cardiac function in dystrophin-deficient mice and Duchenne patient–specific cardiomyocytes by immunoproteasome modulation, *The American Journal of Pathology* (2018), doi: https://doi.org/10.1016/j.ajpath.2018.10.010.

Fibrosis rescue improves cardiac function in dystrophin-deficient mice and Duchenne patient–specific cardiomyocytes by immunoproteasome modulation

Short title: IP inhibition enhances DMD cardiomyopathy

Andrea Farini [1], Aoife Gowran [2], Pamela Bella [1], Clementina Sitzia [3], Alessandro Scopece [2], Elisa Castiglioni [2], Davide Rovina [2], Patrizia Nigro [2], Chiara Villa [1], Francesco Fortunato [4], Giacomo Pietro Comi [4], Giuseppina Milano [2,5], Giulio Pompilio [6,7,8], Yvan Torrente [1]

1 Stem Cell Laboratory, Department of Pathophysiology and Transplantation, Universitá degli Studi di Milano, Unit of Neurology, Fondazione IRCCS Ca' Granda Ospedale Maggiore Policlinico, Centro Dino Ferrari, Milan, Italy

2 Centro Cardiologico Monzino-IRCCS, Unit of Vascular Biology and Regenerative Medicine, Milan, Italy;

3 Scuola di Specializzazione di Patologia Clinica e Biochimica Clinica, Università degli Studi di Milano, struttura di sede: I.R.C.C.S. Policlinico San Donato, UOC SMEL-1

4 Dino Ferrari Centre, Neuroscience Section, Department of Pathophysiology and Transplantation (DEPT), Neurology Unit, IRCCS Foundation Ca' Granda Ospedale Maggiore Policlinico, University of Milan, Via Francesco Sforza 35, 20122, Milan, Italy

5 Laboratory of Cardiovascular Research, Department of Surgery and Anesthesiology, University Hospital of Lausanne, Lausanne, Switzerland

6 Centro Cardiologico Monzino-IRCCS, Unit of Vascular Biology and Regenerative Medicine, Milan, Italy

7 Centro Cardiologico Monzino-IRCCS, Department of Cardiac Surgery, Milan, Italy.

8 Department of Clinical Sciences and Community Health, University of Milan, Italy

Correspondence to: Prof Yvan Torrente, Stem Cell Laboratory, Department of Pathophysiology and Transplantation, Università degli Studi di Milano, Unit of Neurology, Fondazione IRCCS Ca’ Granda Ospedale Maggiore Policlinico, Centro Dino Ferrari, Milan, Italy yvan.torrente@unimi.it

Footnote: A.F. and A.G. contributed equally.

Funding: Supported by Italian Ministry of Health Conte Capitale 2015 (G.P.); Fondazione Umberto Veronesi (A.G.); and Fondazione IEO CCM (D.R.).

Disclosures: None declared.

Abstract

Patients affected by Duchenne muscular dystrophy (DMD) develop a progressive dilated cardiomyopathy characterized by inflammatory cell infiltration, necrosis, and cardiac fibrosis. Standard treatments consider the use of β-blockers and angiotensin-converting enzyme inhibitors that are symptomatic and unspecific towards DMD disease. Medications that target DMD cardiac fibrosis are in early stages of development. Here, we demonstrated immunoproteasome dysregulation in affected hearts of *mdx* mice (murine animal model of DMD) and cardiomyocytes derived from induced pluripotent stem cells of DMD patients. Interestingly, immunoproteasome inhibition ameliorated cardiomyopathy in *mdx* mice and reduced the development of cardiac fibrosis. Establishing the immunoproteasome inhibition–dependent cardioprotective role suggests the possibility to modulate the immunoproteasome as novel and clinically relevant treatment to rescue dilated cardiomyopathy in DMD patients.

Introduction

Skeletal myopathy and muscular dystrophy progression are commonly associated to cardiac dysfunctions and a consequent high mortality due to heart failure [1-3]. In particular, Duchenne muscular dystrophy (DMD) patients present early diastolic dysfunction and myocardial fibrosis that turn into a dilated cardiomyopathy (CM), complicated by heart failure and arrhythmia [4]. Even though recent improvements in the management of respiratory insufficiency have improved the lifespan and overall prognosis of DMD patients, sudden deaths due to heart failure negatively affect their quality of life. A prompt treatment and an early detection of CM represent the requirements for successful cardioprotective therapies that block or at least slowdown the processes of cardiac remodelling and heart failure [3]. Unfortunately, the current treatments for dilated CM are still inadequate since a deep understanding of the specific mechanisms underlying DMD heart failure is lacking. Common approaches are standard and rely on the use of angiotensin-converting enzyme (ACE) inhibitors and β-adrenoceptor antagonists [3]. Most patients with DMD develop cardiomyopathic features between ages 10 and 15 years [4]. Due to this tight timeline during which heart dysfunction appears, DMD offers a unique opportunity to assess strategies to limit cardiomyopathy progression. In the heart of the DMD murine animal model, the *mdx* mouse, from eight weeks of age, the loss of dystrophin, along with membrane integrity, affects calcium (Ca^{2+}) handling and nitric oxide (NO) signalling [5] so that *mdx* cardiomyocytes are susceptible to mechanical stress–induced contractile failure and necrosis [6]. Similarly, in skeletal muscle the lack of dystrophin determines the pathological infiltration of immune cells, such as T lymphocytes and macrophages, and the release of inflammatory cytokines activating nuclear factor-kappa B (NFκB)-dependent pathways [7]. Dilated CM and contractile deviances are evident in 36- to 40-week–old *mdx* mice [8].

Cardiac stress has been recognised for its main role in the up-regulation of inflammatory cytokines/growth factors and the generation of ROS, which modulate different signalling cascades, whose dysfunctions cause altered cytokine secretion and fibrosis commonly affecting dystrophic hearts. In particular the Janus kinase (JAK)–signal transducers and activators of transcription (STAT) can transduce the signal of IL-6/IL-10/interferon gamma (IFN–γ) by means of the selective phosphorylation of STAT1/3 [9]. Similarly, STAT phosphorylation can be driven by different serine kinases, such as p38 mitogen-activated protein kinase (MAPK) and extracellular-regulated kinase (ERK) [9]. In addition, STATs together with NF-κB synergistically up-regulate inducible nitric oxide synthase (iNOS) in DMD muscles, causing the inhibition of the soluble guanylate cyclase 1 alpha (SGC1-α) [10] whereas STAT3 interacts with osteopontin (OPN) in extra-cellular matrix development [11]. In a murine model of hyperglycaemia, it was demonstrated that the proliferative capacity of cardiac fibroblasts and their ability to express collagen was regulated by STAT1/3 possibly through phosphorylated ERK1/2 blockade of collagen expression [12]. Intriguingly, the majority of these proteins/cytokines are deregulated in DMD patients and their functions are commonly influenced by the immunoproteasome (IP).

The IP is formed by the replacement of the catalytic subunits of the constitutive proteasome with other subunits – termed PSMB8, PSMB9, and PSMB10 – that are induced by inflammatory stimuli such as tumor necrosis factor alpha (TNF-α), and interferon (IFN)–γ. Moreover, it is a critical regulator of NFκB signalling driven by selective phosphorylation of STAT1/3 [9]. In the cells of the immune system, the highly expressed IP plays a role in generating peptide ligands for MHC class I antigen presentation [13]. The IP is also present in the heart and is overexpressed in dystrophic muscles [14]. IP up-regulation was observed with concomitant loss of cardiac muscle mass [15], inflammation [16], myocyte atrophy [17] and, in contrast, with over-expression of oxygen species and development of atrial fibrosis [18].

So far, there are several promising IP inhibitors that have been developed and already assessed in phase I/II of clinical trials for selectively treating patients with inflammatory and autoimmune diseases [19,20]. Of note, the potent inhibitor ONX-0914, originally named as PR957 and specifically targeted towards the highly active subunit LMP7 (β5i) of the IP [21], was successfully employed to treat a viral myocarditis by diminishing the expression of pro-inflammatory cytokines/chemokines, reducing infiltration of inflammatory cells, and leading to a general improvement of the cardiac output [22]. In line with this result, our previous work demonstrated that ONX-0914 treatment modulates dystrophic features in *mdx* mice, by reducing the amount of infiltrating activated T cells, myofiber necrosis and collagen deposition in skeletal muscle tissues [23].

The present study confirmed the possibility to use ONX-0914 for inhibiting the IP function, therefore countervailing inflammatory cells and fibrosis in dilated CM of *mdx* mice, and improving their haemodynamic performance. ONX-0914 treatment dampened the release of pro-inflammatory cytokines, decreased MHC-I expression, and increased anti-inflammatory $FoxP3^+$ regulatory T-lymphocytes (T-reg). Considering that early dilated CM is characterized by mild left ventricular dysfunction and differs from advanced dilated CM for left ventricular systolic and diastolic dysfunction, the effect of ONX-0914 treatment was tested in *mdx* mice with early (6 weeks old) and advanced (9 months old) dilated CM. Interestingly ONX-0914 could both counteract the raising of the symptoms of CM in younger *mdx* mice and alleviate the pathology in older *mdx* mice.

Our study underlines the substantial contribution of the IP in infiltrating myocardial immune cells, which actively participate to cardiomyocyte death and successive fibrosis of the DMD heart. Furthermore, the data were translated from *mdx* mice to human cardiomyocytes derived from DMD patients' induced pluripotent stem cells and an aberrant involvement of the IP pathway was detected in dystrophic cardiomyocytes. Based on the present and the previous findings [23], we suggest that the IP possesses a key role directly involved into the poor clinical outcomes observed in DMD patients, therefore representing a promising candidate target for rescuing dystrophic dilated CM.

Materials and Methods

Animal ethics statement

All the procedures performed on living animals are complied with Italian law (D.L.vo 116/92 and subsequent additions) and approved by local ethics committees. This work was authorized by the Ministry of Health and Local University of Milan Committee, authorization number 859/2017-PR (5247B.35, 10/07/2017). Six-week–old (wo) male wild-type (C57Bl), 6wo *mdx* mice and 9-month–old (9mo) *mdx* mice were provided by Charles River. All animals were housed in a controlled ambient environment (12h light/dark cycle) at a temperature between 21 °/23 °C. The mice had free access to clean water and food. Intraperitoneal injection of the IP inhibitor ONX-0914 (Clini Sciences - France, 6mg/Kg) was performed on 6wo and 9mo *mdx* mice for five weeks (two injections per week, *n*=10). Untreated aged-matched *mdx* mice were used as controls.

iPSC generation and characterization

All investigations were conducted following informed consent under regulation of local ethics committee approval (Centro Cardiologico Monzino, Milan, Italy). Human fibroblasts were isolated from dystrophic patients' skin biopsies. Healthy adult dermal fibroblasts were obtained from Tebu-bio and served as controls. Fibroblasts were culture expanded in TMES (Dulbecco's modified Eagle's medium [DMEM] supplemented with 10% HyClone™ fetal bovine serum [GE Healthcare Life Sciences, United Kingdom], 1X MEM Non-Essential Amino Acid Solution, 2mM L-glutamine [both from Stemcell Technologies, Canada] ,and basic fibroblast growth factor [bFGF]). To generate iPSCs, fibroblasts were transfected with four episomal vectors (pCXLE-hUL, pCXLE-hSK, pCXLE-hOCT3/4-shp53-F, and a positive control pCXLE-EGFP) by electroporation (1650 V, 10 ms, 3 pulses) with the Neon™ transfection system (Invitrogen, CA). Transfected fibroblasts were grown on human recombinant vitronectin–coated multi-well plates and maintained in TMES for 48 hr at which point the media was changed to TeSR reprogramming media (Stemcell Technologies) with daily media changes. Emergent iPSC colonies were manually isolated between post transfection days 21 to 30 with a 25G syringe and seeded onto vitronectin-coated multi-well plates in mTeSR1 media (Stemcell Technologies). Fresh medium was replaced daily. From P4 onward iPSCs were passaged without the use of enzymes every three to four days with ReLeSR™ (Stemcell Technologies) and plated as cell aggregates onto vitronectin-coated multi-well plates. Alkaline phosphatase (AP) activity was detected in iPSCs after incubation with AP Live Stain (Invitrogen) for 30 min at 37 ^{o}C. After washing fluorescent-labeled colonies were visualized with a FITC filter and 20X objective (ApoTome, Zeiss, Germany). For the analysis of pluripotency protein expression, stage-specific embryonic antigen-4 (SSEA4) was detected using a commercially available antibody (mouse anti-SSEA4, 1:100 in 5% normal goat

serum (NGS) overnight at 4 °C, Abcam, United Kingdom) and revealed by Alexa Fluor 488 anti-mouse secondary antibody (1:400). Nuclei were counterstained with Hoechst 33342 (Invitrogen). iPSCs were analyzed with FITC filter and 20x objective (LSM710, Zeiss). For FACS analyses, iPSCs were gently dissociated using cell dissociation reagent (Stemcell Technologies) and stained with Tra-1-60 (1:100, 1 h; Abcam). Five percent bovine serum albumin (BSA; Sigma-Aldrich, MO) in PBS was used as blocking solution for excluding non-specific staining (Lonza, Italy). Goat anti-mouse IgM-FITC (1:200, 1 h, Life Technologies) was exploited as secondary antibody. Cells were analyzed using a FACSCalibur™ (BD Biosciences, NJ) or Gallios (Beckman Coulter Life Sciences, IN) flow cytometers.

iPSC cardiomyocyte differentiation and characterization

Cardiomyocyte differentiation of iPSCs was performed following the Lian et al [24] monolayer-directed cardiomyocyte differentiation protocol. Briefly, on Day 0 of differentiation, iPSCs were treated with a GSK3 inhibitor (12µM CHIR99021 in RPMI supplemented with insulin-free B27, Selleck Chemicals LLC, TX, and Invitrogen, respectively). The media was replaced with RPMI supplemented with insulin-free B27 after 24 h. On day 3, a combined media was prepared which contained 1mL conditioned media and 1mL 10µM IWP2 (a Wnt signalling inhibitor, final concentration of 5µM) in RPMI supplemented with insulin-free B27. On day 5, the combined media was replaced with RPMI supplemented with insulin-free B27. On day 7, the media was changed to RPMI supplemented with B27 containing insulin. From this point media was changed every three days. Following 16 days in culture cardiomyocytes derived from human iPSCs (CMs-d-iPSCs) were processed for further analysis. For immunofluorescence analyses of cardiac troponin T type 2 (cTnT2) a commercial cardiomyocyte characterization kit (Life Technologies) was used following the manufacturer's instructions with the exception of secondary antibody used being conjugated to Alexa Fluor 633 (Life Technologies). Cell dissociation reagent (Stemcell Technologies) was used for gently dissociating CM-d-iPSCs for flow cytometry analysis. Afterwards, cells underwent fixation, and permeabilization (BD Biosciences) and blocking using 5% Bovine Serum Albumin (BSA; Sigma-Aldrich) in PBS (Lonza). Cells were stained with an anti-cTnT2 antibody (1:100, 1 hour; Life Technologies) followed by goat anti-mouse IgG1-FITC (1:200, one hour; Life Technologies). Cells were analyzed using a FACS Calibur™ flow cytometer (BD Biosciences). After 14 days of differentiation CMs-d-iPSCs were harvested and plated onto fibronectin-coated multielectrode array (MEA) plates. Cardiac depolarization and repolarization, T waves and field potential durations (FPD) were detected with the Maestro MEA system's cardiac beat detector data processor (Axion BioSystems, GA). Mean FPDs were obtained with the Comprehensive *in vitro* Proarrhythmia Assay (CiPA) analysis tool and plotted using the AxIS Metric plotting Tool (Axion BioSystems).

Modelling DMD cardiomyopathy with patient-specific CMs-d-iPSCs

The determination of dystrophin protein expression in CMs-d-iPSCs by WB was performed by standard techniques using an anti-dystrophin antibody that recognizes human dystrophin (1:500; Abcam) and an anti-GAPDH antibody as a housekeeping protein (1:2000; Abcam). Intracellular free calcium ($[Ca^{2+}]_i$) was determined with a Fluo-4 Calcium Imaging Kit immunofluorescence-based assay kit (Life Technologies) and random images were captured with an ApoTome (Zeiss). Pixel intensity or percent area were calculated using Image J software (https://imagej.nih.gov/ij/; last accessed April 23, 2018). cTnI or TNFα in CMs-d-iPSC–conditioned media was measured with commercial ELISA kits (Life Technologies) and normalized to total protein.

Histological analysis

Animals were sacrificed by cervical dislocation and cardiac muscles of ONX-0914 treated and untreated *mdx* mice were collected for both histological and biochemical analyses. Muscles destined to collagen staining were frozen in liquid-nitrogen–cooled isopentane, and cut on a cryostat (Leica CM1850) into 8 μm. Staining of sections was performed with rabbit anti Collagen I antibody (COL1A1, Cell Signaling Technology, MA). Briefly, heart tissues were blocked for 60 minutes with 3%BSA in PBS at room temperature, and then incubated overnight at 4 °C with primary antibody diluted 1:300 in blocking solution. Monoclonal anti-rabbit 594 (Molecular Probe Invitrogen) was added at dilution 1:200 in blocking solution for one hour. Nuclei were stained with DAPI (Sigma-Aldrich) and images were captured with Leica TCS SP2 confocal microscope. Other animals prior the sacrifice were subjected to cardiac perfusion with saline and followed by a 10% formalin flush. To determine the amount of fibrosis, cardiac tissues were stained by Azan Mallory: the percentage of collagen area per section (stained in blue) was measured by ImageJ software.

Western Blot (WB) analysis

Hearts were isolated from ONX-treated and untreated *mdx* mice and total protein concentration obtained as previously described[25]. Samples were resolved on polyacrylamide gels (ranging from 6% to 12%) and transferred to nitrocellulose membranes (Bio-Rad Laboratories, CA). The membranes were incubated overnight with the primary antibodies against: PSMB5 (1:500; Abcam); PSMB8 (1:500; Abcam); PSMB9 (1:500; Abcam); β tubulin III (1:400; Sigma-Aldrich); vinculin (1:1000; Santa Cruz, TX); OPN (1:500; R&D, MN); FoxP3 (1:500; eBioscience); TNF-α (1:500; eBioscience); TRPC1 (1:500; Santa Cruz); STAT1 (1:400; Cell Signaling Technology); p-STAT1 (1:400; Cell Signaling Technology); STAT-3 (1:400; Cell Signaling Technology); and p-STAT3 (1:400; Cell Signaling Technology). Following incubation, the membranes were detected with peroxidase-conjugated secondary antibodies (Agilent Technologies, CA) and developed by ECL (Amersham Biosciences, United Kingdom).

Mitochondrial enzyme analysis

Cardiac biopsies were collected from ONX-treated and untreated *mdx* mice and the samples were prepared for analysis as previously described[26]. Mitochondrial respiratory chain enzymes and the citrate synthase activities were measured by means of a spectrophotometer as previously described[27]. The value of citrate synthase was used to normalize the values of the other complexes.

RT-qPCR experiments

Total RNA was extracted from cardiac biopsies obtained from ONX-treated and untreated *mdx* mice. cDNA was generated using the Reverse Transcriptase Kit (ThermoFisher Scientific) followed by the SYBR-Green method to quantify the expression of the genes listed in Table 1. All the cDNA samples were tested in duplicate and the threshold cycles (Ct) of target genes were normalized against the glyceraldehyde 3-phosphate dehydrogenase (GAPDH) that was considered a housekeeping gene. Relative transcript levels were calculated from the Ct values as

$$X = 2^{-\Delta ct}$$

where X is the fold difference in amount of target gene versus GAPDH and

$$\Delta Ct = Ct_{target} - Ct_{GAPDH}.$$

Image quantification

Histochemical staining was imaged with an Axioskop II microscope using a digital camera (AxioCamColor) and Axiovision software 4.7 (all by Zeiss), or by a Leica TCS SP2 confocal system, or a Zeiss 710 multiphoton confocal mircroscope with ZEN software version 2010D. Densitometric analyses, manual or automatic counting (Threshold colour Plug-in) were performed using ImageJ Software (http://rsbweb.nih.gov/ij/, version: 2.0.0-rc-2) in 20 sections/muscle.

Statistical analysis and power calculations

Data were analyzed by GraphPad Prism™ and expressed as means±SD or means±SEM. To compare multiple group means, one-way and two-way analysis of variance (ANOVA) were used and multiplicity adjusted *P*-value for each comparison were reported for each analysis. For the comparison of two groups a Student's *t*-test was applied assuming equal variances. The difference among groups was considered significant at $P < 0.05$.

The number of animals per experiment was calculated with the help of the dedicated G POWER online software, considering a power of 80% and a significance level of $P < 0.05$. Based on literature data, the minimum number of animals per experimental group required to observe statistically significant differences is 6 mice/group imaging (ultrasound and haemodynamic) and molecular techniques whereas four mice/group are required for immuno-histochemical analyses, for each timepoint.

Results

ONX-0914 treatment of *mdx* mice affects dilated CM

Following up on the previous work [23], the expression of constitutive proteasome and IP subunits was analyzed by WB in the hearts of 6wo *mdx* mice and C57Bl mice. The results demonstrated that 6wo *mdx* mice over-expressed IP subunits (PSMB8, $P = 0.040$; PSMB9, $P = 0.0491$) whereas the expression of the constitutive proteasome subunit, PSMB5, was not altered (Fig. 1A). To test the efficacy of both early and later stage treatment on DMD cardiac pathology, the effect of ONX-0914 injection was investigated in 6wo and 9mo *mdx* mice: ONX-0914 was administered intra-peritoneally two times/week in 6wo and 9mo *mdx* mice for five weeks followed by transthoracic echocardiography and morphological analysis. In the hearts of *mdx* mice treated with ONX-0914 PSMB8/PSMB9 expression was down-regulated (PSMB8, $P = 0.0184$; PSMB9, $P = 0.0437$) whereas the amount of PSMB5 was unchanged (Fig. 1B). Similarly, in treated-9mo *mdx* mice PSMB8 and PSMB9 were down-regulated (PSMB8, $P = 0.0376$; PSMB9, $P = 0.0093$), whereas the expression of PSMB5 was unaltered (Fig. 1C).

Regarding the transthoracic echocardiography, the aged mdx showed a significant decrease of the ejection fraction (EF) (Two-way ANOVA; $P = 0.0189$) and in the scale stroke volume (SV) (Two-way ANOVA; $P = 0.0034$). However, ONX-0914 treatment induced a significant age-dependent amelioration of EF (Two-way ANOVA; $P = 0.0037$) and stability of SV (Fig. 1D). The ONX0914 treatment resulted in a remarkable reduction left ventricular (LV)-end-systolic/diastolic volumes (LV end-systolic volume [V;s]: Two-way ANOVA; $P = 0.0481$; LV end-diastolic volume [V;d]: Two-way ANOVA; $P = 0.0453$) in ONX-0914-treated 6wo *mdx* compared to untreated age-matched mice (Fig. 1D), Moreover, the ONX0914 treatment did not affect the LV alterations of aged 9mo mdx mice. In addition, following ONX-0914 treatment the 6wo and 9mo *mdx* mice showed significant differences in the length of LV-anterior wall thickness in diastole (LVAW;d) and systole (LVAW;s) and in the length of LV-internal diameter in diastole (LVID;d) and systole (LVID;s) (Fig. 1D). Other echocardiographic measurements revealed significant impairment of cardiac output (CO) ($P = 0.0216$) in ageing mdx but not in ONX-0914–treated age-matched mdx. Length of diameter in diastole (Diameter; d) was stable over time. ONX-0914–treated mdx showed significant differences at nine months compared to six weeks for length of diameter in systole (Diameter;s) ($P = 0.0022$); LV mass

(P = 0.0256); fractional shortening (FS) (P = 0.0011) (Supplemental Fig. S1). These data add to a growing body of literature supporting effects of ONX-0914 in both counteracting the rise of first signs of cardiomyopathy in 6wo *mdx* mice and in alleviating the development of the CM pathology of 9mo *mdx* mice.

ONX0914 treatment diminishes development of fibrosis in 6wo and 9mo *mdx* mice

According to the well-known effects of ONX-0914 on inflammatory cell subpopulations, we hypothesized that our treatment could modify cardiac fibrosis and/or inflammation. Azan Mallory staining of LV/RV and of interventricular septum revealed that 9mo *mdx* mice were largely characterized by disorganized cardiomyocytes, prominent myocardial interstitial and perivascular fibrosis whereas younger 6wo *mdx* showed mild substantial myocardial deterioration and fibrotic deposition (Fig. 1E, F). The ONX-0914 reduced significantly most signs of cardiac fibrosis in 6wo (Fig. 1E; P = 0.0180) and 9mo (Fig. 1F; P = 0.0023) *mdx* mice with comparatively mild perivascular fibrosis in the LV and interventricular septum, and perivascular-restricted fibrous deposition in the RV, thus agreeing with the functional benefits of ONX-0914 treatment for dystrophic myocardium.

Further, the level of the mediator of fibrosis as OPN (Fig. 2A-D; P = 0.0299 and P = 0.1510 respectively) and phosphorylation of ERK1/2 (Fig. 2A-D; for pERK1/2 P = 0.0003 and P = 0.0370, respectively) were significantly depressed in ONX-0914 treated hearts of 6wo and 9mo *mdx* mice. As OPN can interact with STAT proteins [28] and STAT-dependent pathways commonly regulate IP structure and function [29, 30], the expression of these proteins to uncover potential IP-dependent molecular mechanisms regulating pathological fibrosis was investigated in *mdx* CM. Following ONX-0914 treatment, the ratios between both total and phosphorylated STAT1 and STAT3 were significantly down-regulated (Fig. 2A, B; P = 0.0276 and P = 0.0194 for pSTAT3/STAT3 and pSTAT1/STAT1, respectively). As in younger *mdx* mice, treated 9mo *mdx* showed a significant down-regulation of the ratio between both total and phosphorylated STAT1 (Fig. 2C, D; P = 0.0469). Decreased levels of COL1A (Fig. 2E) and collagen 3a (Fig. 2F; P = 0.0085 and P = 0.2477 for 6wo and 9mo *mdx*, respectively) found in ONX-0914–treated hearts of *mdx* mice agree with the observed differences in fibrosis.

ONX-0914 down-regulated the inflammatory responses in 6wo and 9mo *mdx* mice

Accordingly with modifications in the extent of fibrosis, the amount of pro-inflammatory cytokines expressed in cardiac samples from treated and untreated 6wo *mdx* mice were determined: RT-qPCR experiments proved that the pro-inflammatory cytokines IL-1β and TNF-α were over-expressed in 6wo untreated *mdx* mice compared to ONX-treated ones (Fig. 3A; P = 0.0250 for IL-1β and P = 0.151 for TNF-α). Thus, the amount of immune infiltrating cells that normally secrete pro-inflammatory IL-1β and TNF-α was evaluated and significant reduction of these cells (ranging

from 10 to more than 100 cells) was found in ONX-0914–treated 6wo *mdx* hearts (Fig. 3B). Interestingly, the $CD3^+CD45^+$ subpopulation (B- and T-lymphocytes) was significantly decreased in ONX-0914–treated hearts of 6wo *mdx* ($P < 0.01$) whereas no differences in the percentage of CD107 positive macrophages was found (data not shown). The specific reduction of B- and T-lymphocytes upon IP inhibition was corroborated by detection of significantly reduced MHC-I expression (Fig. 3C; $P = 0.0387$) and over-expression of FoxP3, the specific marker of Tregs that act to suppress immune response (Fig. 3C; $P = 0.0357$). Additionally, RT-qPCR experiments revealed that ONX-0914 treatment reduced the expression of retinoic acid receptor–related orphan receptor gamma (ROR-γt), a master regulator of pro-inflammatory Th17 lymphocytes (Fig. 3D; $P = 0.0472$) and macrophage-specific marker chemokine C-C motif ligand 2 (CCL2) (Fig. 3D; $P = 0.0212$) in hearts of 6wo *mdx* mice.

Similar to pathological features described in 6wo *mdx* mice, in 9mo *mdx* mice a down-regulation of ROR-γt ($P = 0.0414$) and CCL2 (Fig. 3E) was seen and ONX-0914 treatment was found to diminish the amount of TNF-α (Fig. 3F). These evidences suggest that overwhelming immune-cell and cytokine reduction was significant at detectible onset of cardiac functional decline whereas reduced fibrosis, improved diastolic filling, and amelioration of cardiac output were equally present in both prior and advanced decline.

ONX-0914 affects cardiac mitochondrial functions only in 9mo *mdx* mice

According to several works, DMD tissues display a deficit in resting ATP levels [32], consequently, it was reported that active mitochondria were necessary to rescue sarcolemmal abnormalities in myofibers [33]. To determine whether the diminished fibrosis was partially due to an amelioration of the amount/functionality of mitochondria, several mitochondrial enzymes were studied in the hearts of ONX-treated and untreated 6wo and 9mo *mdx* mice. As expected, two-ANOVA analysis revealed increased mitochondrial activity in aged *mdx* mice with significant up-regulation of NADH dehydrogenase (DH) ($P = 0.0140$), NADH cytochrome-C reductase ($P = 0.008$), succinate cytochrome-C reductase ($P = 0.0007$), and cytochrome oxidase ($P < 0.0001$) (Supplemental Fig. S2A). Conversely, ONX-0914 treatment of 9mo *mdx* mice determined significant reduction of the enzymatic activity of NADH cytochrome-C reductase ($P = 0.0337$) and, in particular, of succinate cytochrome-C reductase ($P = 0.0009$) and cytochrome oxidase ($P < 0.0001$) (Supplemental Fig. S2A), thus resembling the values of 6wo *mdx* mice. Since the abnormal cytosolic Ca^{2+} levels present in mdx cardiomyocytes lead to an age-dependent degeneration of mitochondrial structure and function [34], the expression of the transient receptor potential channel was evaluated for calcium (TRPC1). Although TRPC1 is up-regulated in *mdx* hearts confirming previous evidences [35], no differences were found between ONX-0914–treated and untreated 6wo and 9mo *mdx* mice (Supplemental Fig. S2B).

Cardiomyocytes derived from dystrophic iPSCs recapitulate abnormal IP expression as observed in *mdx* mice

As it is extremely difficult to obtain cardiac biopsies from muscular dystrophy patients, to confirm the interesting results derived from *mdx* mice, human dermal fibroblasts (HDFs) were reprogrammed with non-integrating episomal vectors containing the 'Yamanaka factors' [36] (Fig. 4A). Several lines of iPSCs were established from healthy controls (CTR) and DMD patients under feeder-free defined conditions [37], which displayed pluripotent morphology and expressed alkaline phosphatase, SSEA4 and Tra-1-60, as assessed by immunofluorescence and FACS (Fig. 4B; 87±8 vs 83%±13 % Tra-1-60 positive cells). Cardiomyocytes were derived from CTR and DMD iPSC lines (CMs-d-iPSCs) through the temporal modulation of Wnt signalling in iPSCs grown in defined feeder-free monolayers as already described elsewhere[24]. There was no significant difference in the percentage of cardiac troponin T type 2 (cTnT2) positive cells (Fig. 4C; 92±1 vs 81%±14 % $cTnT2^+$ cells). CMs-d-iPSCs displayed spontaneous beating with electrical activity similar to other reports in the literature[38, 39] (Fig. 4D-G). Interestingly, through Poincare Plot the absence of unstable/abnormal beats as in arrhythmias was also determined (Fig. 4H). CMs-d-iPSCs were maintained as beating monolayers until day 16 of cardiomyocyte differentiation followed by the assessment of DMD cardiac disease hallmarks. An up-regulation of intracellular free calcium ($[Ca^{2+}]_i$) in DMD CMs-d-iPSCs but not in CTR CMs-d-iPSCs was observed (Fig. 5A; 1162±33 vs 1530±45 mean pixel intensity, $P < 0.0001$), which correlates with our previous observation of increased function of voltage-gated calcium (Cav1) channels association with DMD-CM pathophysiological alterations [40]. In DMD CMs-d-iPSCs full-length dystrophin protein was absent in comparison to CTR CMs-d-iPSCs (Fig. 5B). Furthermore, DMD CMs-d-iPSCs recapitulated relevant clinical characteristics of DMD, as they displayed increased release of the cardiac damage marker cardiac troponin I (cTnI; Fig. 5C; 0.65±0.10 vs 1.92±0.35 ng cTnI per mg total protein, $P = 0.0072$) and of TNF-α (-0.8128 ± 0.2386 vs 3.358 ± 1.705). The expression of constitutive and IP subunits in the CMs-d-iPSCs was determined. The PSMB5 subunit remained unaltered in DMD CMs-d-iPSCs), the IP subunits PSMB8 ($P = 0.0417$) and PSMB9 ($P = 0.0377$) were significantly over-expressed in DMD CMs-d-iPSCs compared to CTR CMs-d-iPSCs (Fig. 6A). Next, the effect of ONX-0914 treatment was monitored on CM hallmarks. Significantly, IP inhibition dampened $[Ca^{2+}]_i$ ($P < 0.0001$ for both DMD CMs and DMD CMs+ONX-0914 versus CTR CMs; 1-way ANOVA) (Fig. 6B) and also reduced the release of cTnI related to DMD CMs (with $P = 0.0013$, $P = 0.0094$, $P = 0.0399$ for CTR CMs, CTR CMs+ONX, DMD CMs+ONX, respectively; two-way ANOVA) (Fig. 6C). Interestingly, RT-qPCR demonstrated the down-regulation of TGF-β and collagen-3a expression in treated CMs-d-iPSCs ($P = 0.0235$ and $P = 0.0020$, respectively) (Fig. 6D). CTR and DMD CMs-d-iPSCs treated with 200nM ONX-0914 displayed a severe acute cardiotoxic response which was not observed at concentrations <150nM demonstrating a dose-dependent toxic pattern in CMs-d-iPSCs. Specifically, two days post-treatment, CMs-d-

iPSCs started displaying abnormal behavior and were on visual inspection of a distinct poorer quality to vehicle-treated CMs-d-iPSCs. After three to four days of treatment, most CMs-d-iPSCs stopped contracting and displayed a further deterioration in cellular morphology. Following seven days of treatment, the majority of CMs-d-iPSCs were detached and necrotic (Supplemental Fig. S3A) and the few remaining CMs-d-iPSCs displayed overt aberrations in morphology (Supplemental Fig. S3B-D).

Discussion

Dilated CM is the major cause of death of DMD patients and is predominantly characterized by severe inflammation and fibrosis. Unfortunately, dilated CM is unresponsive to usual care based on glucocorticoids [41,42], increasing the urgencies for novel treatments aimed at improving the poor DMD clinical outcomes and preventing fatal heart failure. The murine model of DMD, the *mdx* mouse, develops dilated CM by 32 weeks of age, when accumulation of connective tissue and contractile deviances are undeniable [43]. However, contractile dysfunctions and development of ventricular inflammation and fibrosis have already been described in *mdx* mice as early as two months of age [6,7]. IP functions are synergistically associated with the activity of most of the proteins that are involved in the development of the symptoms that will lead to dilated CM such as cardiomyocyte necrosis, myocardial tissue degeneration, and fibrosis [22,44,45]. Here we demonstrated the overexpression of IP subunits in *mdx* hearts and suggested IP modulation as a valuable tool to counteract cardiac pathology in *mdx* mice.

The IP inhibition by ONX-0914 treatment decreased inflammatory cell activation, pro-inflammatory cytokine expression, and fibrosis and ameliorated the haemodynamic performance of *mdx* with early (6wo) and advanced (9mo) dilated CM. Interestingly, IP modulation determines the delay of cardiomyopathy in *mdx* with early dilated CM (6wo) and improves the cardiac performance of older *mdx* with advanced dilated CM (9mo). LV dysfunction was prominent in untreated 9mo mdx. ONX-0914 administration prior to the onset of cardiac functional decline preserved LV systolic function (ie, ejection fraction and wall thickness). Improvements in *mdx* heart histology resulted from the treatment correlated well with the functional improvements detected by echocardiography. Outstandingly, inhibition of PSMB8 in 6wo *mdx* mice down-regulated the expression of pERK1/2 that potentially phosphorylate STATs and thus control collagen expression (whose deposition is typical of myocardial fibrosis). Importantly, ONX-0914 treatment reduced the percentage of infiltrating B- and T-cells in *mdx* hearts which in turn cause the down-regulation of NFκB, hampering its cooperation with STATs. Such effects may also be attributed to the reduced expression of inflammatory cytokines such as ROR-γt, IL-1β, and TNF-α that activate the JAK/STAT pathways. Interestingly, a down-regulation of the fibrotic enhancer OPN and decreased levels of collagen 1a and 3a that agree with the observed differences in fibrosis of ONX-0914 treated *mdx* mice, were observed. These data are in accordance with those published by other groups

demonstrating the immunomodulatory role of OPN in DMD [46] and its relationship with matrix metallo-proteinase 9 (MMP9) [47]. Recently, in a cohort of 40 DMD patients with early myocardial disease, Raman et al showed a combinatorial effect of ACEI and ARB with the drug Eplerenone (commonly used in the management of chronic heart failure), which improved cardiac features possibly through a modulation of an OPN-dependent pathway [48]. Thus we propose OPN as a reliable target to ameliorate cardiac fibrosis in DMD [49]. Nevertheless, the reduced inflammatory activation and fibrosis obtained in ONX-0914–treated hearts of *mdx* mice leads to improved haemodynamic performance characterized by increased LV ejection fraction and decreased LV-end-systolic/diastolic volumes. Since substantial improvement of dilated CM was observed in ONX-0914–treated *mdx* mice, it was analyzed whether the same effect could be translated to DMD. Thus, dermal fibroblasts isolated from DMD patients and healthy individuals were reprogrammed to iPSCs which were then differentiated to functional beating CMs-d-iPSCs. It was confirmed that DMD CMs-d-iPSCs over-expressed the IP subunits and their inhibition protected cardiomyocytes from damage as indicated by decreased release of cTnI and TNF-α. In addition the anti-fibrotic function of ONX-0914—at a non-toxic concentration of 150nM, as cardiotoxicity was determined when ONX-0914 was used at 200nM—could be exerted through down-regulation of TGF-β and collagen-1a expression. Interestingly, in an animal model of hypertension, the over-expression of the IP subunit PSMB10 was found to be responsible for increasing atrial fibrosis through TGF-β/SMAD2/3 pathways and for the up-regulation of inflammation and oxidative stress mediated by NF-kB [18].

Taken together these data demonstrate the beneficial effects of ONX-0914 to treat and prevent DCM of *mdx* mice ranking the IP inhibitor compounds among the novel drugs to be tested in future DMD clinical trials [50, 51].

Acknowledgments

We thank the Associazione Amici del Centro Dino Ferrari.

Y.T., G.P., A.F., and C.S. conceived and designed the experiments. C.S., A.F., and A.G. wrote the paper. A.F., A.G., P.N., and C.G.P. interpreted and analyzed the data. M.G., E.C., D.R., A.S., B.P., and F.F. performed the experiments.

References

[1] Beynon RP, Ray SG: Cardiac involvement in muscular dystrophies. QJM : monthly journal of the Association of Physicians 2008, 101:337-44.

[2] Judge DP, Kass DA, Thompson WR, Wagner KR: Pathophysiology and therapy of cardiac dysfunction in Duchenne muscular dystrophy. American journal of cardiovascular drugs : drugs, devices, and other interventions 2011, 11:287-94.

[3] Verhaert D, Richards K, Rafael-Fortney JA, Raman SV: Cardiac involvement in patients with muscular dystrophies: magnetic resonance imaging phenotype and genotypic considerations. Circulation Cardiovascular imaging 2011, 4:67-76.

[4] Kamdar F, Garry DJ: Dystrophin-Deficient Cardiomyopathy. Journal of the American College of Cardiology 2016, 67:2533-46.

[5] Williams IA, Allen DG: Intracellular calcium handling in ventricular myocytes from mdx mice. American journal of physiology Heart and circulatory physiology 2007, 292:H846-55.

[6] Danialou G, Comtois AS, Dudley R, Karpati G, Vincent G, Des Rosiers C, Petrof BJ: Dystrophin-deficient cardiomyocytes are abnormally vulnerable to mechanical stress-induced contractile failure and injury. FASEB journal : official publication of the Federation of American Societies for Experimental Biology 2001, 15:1655-7.

[7] Nakamura A, Yoshida K, Takeda S, Dohi N, Ikeda S: Progression of dystrophic features and activation of mitogen-activated protein kinases and calcineurin by physical exercise, in hearts of mdx mice. FEBS letters 2002, 520:18-24.

[8] Quinlan JG, Hahn HS, Wong BL, Lorenz JN, Wenisch AS, Levin LS: Evolution of the mdx mouse cardiomyopathy: physiological and morphological findings. Neuromuscular disorders : NMD 2004, 14:491-6.

[9] Barry SP, Townsend PA, Latchman DS, Stephanou A: Role of the JAK-STAT pathway in myocardial injury. Trends in molecular medicine 2007, 13:82-9.

[10] Xuan YT, Guo Y, Han H, Zhu Y, Bolli R: An essential role of the JAK-STAT pathway in ischemic preconditioning. Proceedings of the National Academy of Sciences of the United States of America 2001, 98:9050-5.

[11] Hilfiker-Kleiner D, Hilfiker A, Fuchs M, Kaminski K, Schaefer A, Schieffer B, Hillmer A, Schmiedl A, Ding Z, Podewski E, Podewski E, Poli V, Schneider MD, Schulz R, Park JK, Wollert KC, Drexler H: Signal transducer and activator of transcription 3 is required for myocardial capillary growth, control of interstitial matrix deposition, and heart protection from ischemic injury. Circ Res 2004, 95:187-95.

[12] Dai B, Cui M, Zhu M, Su WL, Qiu MC, Zhang H: STAT1/3 and ERK1/2 synergistically regulate cardiac fibrosis induced by high glucose. Cellular physiology and biochemistry : international journal of experimental cellular physiology, biochemistry, and pharmacology 2013, 32:960-71.

[13] Ebstein F, Kloetzel PM, Kruger E, Seifert U: Emerging roles of immunoproteasomes beyond MHC class I antigen processing. Cellular and molecular life sciences : CMLS 2012, 69:2543-58.

[14] Chen CN, Graber TG, Bratten WM, Ferrington DA, Thompson LV: Immunoproteasome in animal models of Duchenne muscular dystrophy. Journal of muscle research and cell motility 2014, 35:191-201.

[15] Zu L, Bedja D, Fox-Talbot K, Gabrielson KL, Van Kaer L, Becker LC, Cai ZP: Evidence for a role of immunoproteasomes in regulating cardiac muscle mass in diabetic mice. J Mol Cell Cardiol 2010, 49:5-15.

[16] Opitz E, Koch A, Klingel K, Schmidt F, Prokop S, Rahnefeld A, Sauter M, Heppner FL, Volker U, Kandolf R, Kuckelkorn U, Stangl K, Kruger E, Kloetzel PM, Voigt A: Impairment of immunoproteasome function by beta5i/LMP7 subunit deficiency results in severe enterovirus myocarditis. PLoS pathogens 2011, 7:e1002233.

[17] Cosper PF, Harvey PA, Leinwand LA: Interferon-gamma causes cardiac myocyte atrophy via selective degradation of myosin heavy chain in a model of chronic myocarditis. The American journal of pathology 2012, 181:2038-46.

[18] Li J, Wang S, Bai J, Yang XL, Zhang YL, Che YL, Li HH, Yang YZ: Novel Role for the Immunoproteasome Subunit PSMB10 in Angiotensin II-Induced Atrial Fibrillation in Mice. Hypertension 2018.

[19] Basler M, Mundt S, Bitzer A, Schmidt C, Groettrup M: The immunoproteasome: a novel drug target for autoimmune diseases. Clinical and experimental rheumatology 2015, 33:S74-9.

[20] Mundt S, Basler M, Buerger S, Engler H, Groettrup M: Inhibiting the immunoproteasome exacerbates the pathogenesis of systemic Candida albicans infection in mice. Scientific reports 2016, 6:19434.

[21] Muchamuel T, Basler M, Aujay MA, Suzuki E, Kalim KW, Lauer C, Sylvain C, Ring ER, Shields J, Jiang J, Shwonek P, Parlati F, Demo SD, Bennett MK, Kirk CJ, Groettrup M: A selective inhibitor of the immunoproteasome subunit LMP7 blocks cytokine production and attenuates progression of experimental arthritis. Nature medicine 2009, 15:781-7.

[22] Althof N, Goetzke CC, Kespohl M, Voss K, Heuser A, Pinkert S, Kaya Z, Klingel K, Beling A: The immunoproteasome-specific inhibitor ONX 0914 reverses susceptibility to acute viral myocarditis. EMBO molecular medicine 2018.

[23] Farini A, Sitzia C, Cassani B, Cassinelli L, Rigoni R, Colleoni F, Fusco N, Gatti S, Bella P, Villa C, Napolitano F, Maiavacca R, Bosari S, Villa A, Torrente Y: Therapeutic Potential of Immunoproteasome Inhibition in Duchenne Muscular Dystrophy. Molecular therapy : the journal of the American Society of Gene Therapy 2016.

[24] Lian Q, Zhang Y, Zhang J, Zhang HK, Wu X, Zhang Y, Lam FF, Kang S, Xia JC, Lai WH, Au KW, Chow YY, Siu CW, Lee CN, Tse HF: Functional mesenchymal stem cells derived from human induced pluripotent stem cells attenuate limb ischemia in mice. Circulation 2010, 121:1113-23.

[25] Parolini D, Meregalli M, Belicchi M, Razini P, Lopa R, Del Carlo B, Farini A, Maciotta S, Bresolin N, Porretti L, Pellegrino M, Torrente Y: CD20-related signaling pathway is differently activated in normal and dystrophic circulating CD133(+) stem cells. Cellular and molecular life sciences : CMLS 2009, 66:697-710.

[26] Sitzia C, Farini A, Colleoni F, Fortunato F, Razini P, Erratico S, Tavelli A, Fabrizi F, Belicchi M, Meregalli M, Comi G, Torrente Y: Improvement of endurance of DMD animal model using natural polyphenols. BioMed research international 2015, 2015:680615.

[27] Bresolin N, Zeviani M, Bonilla E, Miller RH, Leech RW, Shanske S, Nakagawa M, DiMauro S: Fatal infantile cytochrome c oxidase deficiency: decrease of immunologically detectable enzyme in muscle. Neurology 1985, 35:802-12.

[28] Behera R, Kumar V, Lohite K, Karnik S, Kundu GC: Activation of JAK2/STAT3 signaling by osteopontin promotes tumor growth in human breast cancer cells. Carcinogenesis 2010, 31:192-200.

[29] Ferrington DA, Gregerson DS: Immunoproteasomes: structure, function, and antigen presentation. Progress in molecular biology and translational science 2012, 109:75-112.

[30] Pickering AM, Koop AL, Teoh CY, Ermak G, Grune T, Davies KJ: The immunoproteasome, the 20S proteasome and the PA28alphabeta proteasome regulator are oxidative-stress-adaptive proteolytic complexes. Biochem J 2010, 432:585-94.

[31] Kuswanto W, Burzyn D, Panduro M, Wang KK, Jang YC, Wagers AJ, Benoist C, Mathis D: Poor Repair of Skeletal Muscle in Aging Mice Reflects a Defect in Local, Interleukin-33-Dependent Accumulation of Regulatory T Cells. Immunity 2016, 44:355-67.

[32] Cole MA, Rafael JA, Taylor DJ, Lodi R, Davies KE, Styles P: A quantitative study of bioenergetics in skeletal muscle lacking utrophin and dystrophin. Neuromuscular disorders : NMD 2002, 12:247-57.

[33] Vila MC, Rayavarapu S, Hogarth MW, Van der Meulen JH, Horn A, Defour A, Takeda S, Brown KJ, Hathout Y, Nagaraju K, Jaiswal JK: Mitochondria mediate cell membrane repair and contribute to Duchenne muscular dystrophy. Cell death and differentiation 2016.

[34] Kyrychenko V, Polakova E, Janicek R, Shirokova N: Mitochondrial dysfunctions during progression of dystrophic cardiomyopathy. Cell calcium 2015, 58:186-95.

[35] Shirokova N, Niggli E: Cardiac phenotype of Duchenne Muscular Dystrophy: insights from cellular studies. J Mol Cell Cardiol 2013, 58:217-24.

[36] Okita K, Matsumura Y, Sato Y, Okada A, Morizane A, Okamoto S, Hong H, Nakagawa M, Tanabe K, Tezuka K, Shibata T, Kunisada T, Takahashi M, Takahashi J, Saji H, Yamanaka S: A more efficient method to generate integration-free human iPS cells. Nature methods 2011, 8:409-12.

[37] Spaltro G, Vigorelli V, Casalnuovo F, Spinelli P, Castiglioni E, Rovina D, Paganini S, Di Segni M, Nigro P, Gervasini C, Pompilio G, Gowran A: Derivation of the Duchenne muscular dystrophy patient-derived induced pluripotent stem cell line lacking DMD exons 49 and 50 (CCMi001DMD-A-3, 49, 50). Stem cell research 2017, 25:128-31.

[38] Izumi-Nakaseko H, Nakamura Y, Wada T, Ando K, Kanda Y, Sekino Y, Sugiyama A: Characterization of human iPS cell-derived cardiomyocyte sheets as a model to detect drug-induced conduction disturbance. The Journal of toxicological sciences 2017, 42:183-92.

[39] Nakamura Y, Matsuo J, Miyamoto N, Ojima A, Ando K, Kanda Y, Sawada K, Sugiyama A, Sekino Y: Assessment of testing methods for drug-induced repolarization delay and arrhythmias in an iPS cell-derived cardiomyocyte sheet: multi-site validation study. Journal of pharmacological sciences 2014, 124:494-501.

[40] Nanni S, Re A, Ripoli C, Gowran A, Nigro P, D'Amario D, Amodeo A, Crea F, Grassi C, Pontecorvi A, Farsetti A, Colussi C: The nuclear pore protein Nup153 associates with chromatin and regulates cardiac gene expression in dystrophic mdx hearts. Cardiovascular research 2016, 112:555-67.

[41] Markham LW, Kinnett K, Wong BL, Woodrow Benson D, Cripe LH: Corticosteroid treatment retards development of ventricular dysfunction in Duchenne muscular dystrophy. Neuromuscular disorders : NMD 2008, 18:365-70.

[42] Marques MJ, Oggiam DS, Barbin IC, Ferretti R, Santo Neto H: Long-term therapy with deflazacort decreases myocardial fibrosis in mdx mice. Muscle & nerve 2009, 40:466-8.

[43] Spurney CF, Knoblach S, Pistilli EE, Nagaraju K, Martin GR, Hoffman EP: Dystrophin-deficient cardiomyopathy in mouse: expression of Nox4 and Lox are associated with fibrosis and altered functional parameters in the heart. Neuromuscular disorders : NMD 2008, 18:371-81.

[44] Chen S, Kammerl IE, Vosyka O, Baumann T, Yu Y, Wu Y, Irmler M, Overkleeft HS, Beckers J, Eickelberg O, Meiners S, Stoeger T: Immunoproteasome dysfunction augments alternative polarization of alveolar macrophages. Cell death and differentiation 2016, 23:1026-37.

[45] Yan W, Bi HL, Liu LX, Li NN, Liu Y, Du J, Wang HX, Li HH: Knockout of immunoproteasome subunit beta2i ameliorates cardiac fibrosis and inflammation in DOCA/Salt hypertensive mice. Biochemical and biophysical research communications 2017, 490:84-90.

[46] Vetrone SA, Montecino-Rodriguez E, Kudryashova E, Kramerova I, Hoffman EP, Liu SD, Miceli MC, Spencer MJ: Osteopontin promotes fibrosis in dystrophic mouse muscle by modulating immune cell subsets and intramuscular TGF-beta. The Journal of clinical investigation 2009, 119:1583-94.

[47] Dahiya S, Givvimani S, Bhatnagar S, Qipshidze N, Tyagi SC, Kumar A: Osteopontin-stimulated expression of matrix metalloproteinase-9 causes cardiomyopathy in the mdx model of Duchenne muscular dystrophy. Journal of immunology 2011, 187:2723-31.

[48] Raman SV, Hor KN, Mazur W, Halnon NJ, Kissel JT, He X, Tran T, Smart S, McCarthy B, Taylor MD, Jefferies JL, Rafael-Fortney JA, Lowe J, Roble SL, Cripe LH: Eplerenone for early cardiomyopathy in Duchenne muscular dystrophy: a randomised, double-blind, placebo-controlled trial. Lancet Neurol 2015, 14:153-61.

[49] Kharraz Y, Guerra J, Mann CJ, Serrano AL, Munoz-Canoves P: Macrophage plasticity and the role of inflammation in skeletal muscle repair. Mediators of inflammation 2013, 2013:491497.

[50] Bauer R, Straub V, Blain A, Bushby K, MacGowan GA: Contrasting effects of steroids and angiotensin-converting-enzyme inhibitors in a mouse model of dystrophin-deficient cardiomyopathy. European journal of heart failure 2009, 11:463-71.

[51] Guerron AD, Rawat R, Sali A, Spurney CF, Pistilli E, Cha HJ, Pandey GS, Gernapudi R, Francia D, Farajian V, Escolar DM, Bossi L, Becker M, Zerr P, de la Porte S, Gordish-Dressman H, Partridge T, Hoffman EP, Nagaraju K: Functional and molecular effects of arginine butyrate and prednisone on muscle and heart in the mdx mouse model of Duchenne Muscular Dystrophy. PLoS One 2010, 5:e11220.

Figure Legends

Figure 1. Expression of IP in C57Bl, *mdx*, and ONX-0914–treated *mdx* mice and evaluation of IP inhibition in *mdx* mice. Representative measurement of the expression of IP subunits. WB analysis reveals over-expression of IP subunits PSMB8 and PSMB9 in 6wo *mdx* hearts related to C57Bl (**A**) and demonstrates that treatment with ONX-0914 down-regulates IP expression in 6wo *mdx* mice (**B**). Similar down-regulation of IP subunits amount is evidenced in 9mo *mdx* mice treated with ONX-0914 (**C**). Transthoracic echocardiography shows that ONX-0914–treated 6wo *mdx* mice have significant decrease of LV end-systolic and diastolic volumes with significant improvement of LV ejection fraction, whereas ONX-0914–treated 9mo *mdx* mice up-regulate SV and LVAW;s (**D**). Representative Azan Mallory images of LV of ONX-0914–treated and untreated 6wo (**E**) and 9mo (**F**) *mdx* mice. Histogram represents the percentage of cardio-fibrotic area per section of treated and untreated *mdx* mice (n=3 animals per group) (**E** and **F**). Scale bar=200μm. Data are presented as mean ± SEM of n=3 (**A**); n=3 to 5 (**B**, **C**); n=5 to 8 (**D**) independent experiments. Statistical analysis was performed by Student *t*-test (**A, B, C, E, F:** †$P < 0.05$ vs C57Bl; *$P < 0.05$, **$P < 0.01$ vs *mdx*) and two-way ANOVA (**D:** ‡$P < 0.05$, ‡‡$P < 0.01$, and ‡‡‡$P < 0.001$). EF= ejection fraction. V;s= LV end-systolic volume. V;d= LV end-diastolic volume. LVAW;d= Left ventricular anterior wall thickness in diastole. LVAW;s= Left ventricular anterior wall thickness in systole. LVID;d= Left ventricular internal diameter in diastole. LVID;s= Left ventricular internal diameter in systole. nSV= scaled stroke volume.

Figure 2. Amelioration of fibrotic mediators in *mdx* mice following ONX-0914 treatment. Measurement of the expression of pivotal pro-fibrotic proteins in 6wo *mdx* mice by WB analysis (**A**). Down-regulation of the pSTAT1/STAT1 and pSTAT3/STAT3 ratios and OPN and pERK1/2 in ONX-0914 treated 6wo *mdx* mice (**B**). In 9mo *mdx* mice a similar down-regulation of pERK1/2 and pSTAT1/STAT1 ratio is seen whereas OPN variation is not significant (**C, D**). Immunofluorescence staining reveals that ONX-0914 treatment determines the down-regulation of collagen 1a (COL1A) (in red) expression in both 6wo and 9mo *mdx* mice (representative images of LV) (**E**; scale bar=50μm). RT-qPCR experiments demonstrate a decrease in collagen 3a gene transcript in 6wo and 9mo *mdx* mice (**F**). Data are presented as mean ± SEM of n=3 (**A, B, C, D**) and n=6 (**F**) independent experiments. Student *t*-test: *$P < 0.05$, **$P < 0.01$, and ****$P < 0.0001$ vs *mdx*.

Figure 3. IP inhibition down-regulates inflammatory mediators in *mdx* mice. RT-qPCR experiments show a down-regulation of pro-inflammatory cytokines IL-1β and TNF-α in 6wo *mdx* mice (**A**). H&E staining of 6wo *mdx* heart tissue sections demonstrates the reduction of the infiltrating cells in LV of treated mice (**B**), whereas there is an over-expression of the FoxP3 protein and a slight but significant decrease in MHC-I (**C**). *RORγt* and *CCL2* expression is down-regulated in ONX-treated 6wo *mdx* mice as assessed by RT-qPCR experiments (**D**). In older *mdx* mice, *RORγt* expression is down-regulated whereas *CCL2* amount is reduced but not significant (**E**). WB analysis shows that TNFα is down-regulated in ONX-treated 9mo *mdx* mice (**F**). Data are presented as mean ± SEM of n=6 (**A**) and n=3 (**C, D, E**) independent experiments. Student t-test: $*P < 0.05$ vs *mdx*.

Figure 4. Derivation of cardiomyocytes from dystrophic patients' induced pluripotent stem cells. Reprogramming of human dermal fibroblasts by transfection via electroporation with episomal vectors containing the 'Yamanaka factors'. Scale bar=100μm/50μm/100μm/200μm, respectively (**A**, black arrow indicates the mesenchymal-to-epithelial transition phase of the reprogramming process). Immunohistochemical characterization of iPSCs for alkaline phosphatase activity and expression of SSEA4 and Tra-1-60 by immunohistochemistry and FACS analyses, respectively, in CTR/DMD iPSCs lines. Scale bar=100μm. (**B**). Generation of high percentages of $cTnT2^{+}$ CMs-d-iPSCs from CTR and DMD iPSC lines through modulation of Wnt signaling in iPSCs. Scale bar=100μm (**C**). Replated CMs-d-iPSCs re-develop spontaneous beating 2 days after plating onto MEA plates. Scale bar=100μm (**D**). Continuous voltage and conduction data were recorded for 2 minutes by the Maestro's cardiac beat detector (**E**). Conduction propagation pattern of a well showing the spike arrival times of the initiation (blue) and termination (red) of a synchronized beat (black circles indicate that a beat was not detected on that electrode and x- and y-axis represent electrode column and row numbers) (**F**). Beat waveforms from all electrodes were vertically aligned (black lines) followed by selection of the "Golden electrode" (blue line, defined as an electrode with a repolarization traceable across all conditions and is the electrode used for field potential duration [FPD] analysis) for each well. Mean FPDs over the entire plate were calculated and plotted (G, red verticle line represents the "Golden Channel" T-wave peak). A Poincaré plot showed no discernible arrhythmic events (green circles indicate those beats used for calculating the average beat waveform for the FDP detection) (**H**). All analyses were performed using the CiPA analysis tool. Data are presented as mean ± SEM of n=3 (**B**) and n=4 (**C**) independent experiments.

Figure 5. Characterization of MD cardiomyopathy hallmarks in patients' specific CMs-d-iPSCs. Representative staining of CTR and DMD cardiomyocytes with the green fluorescent calcium indicator Flou-4 AM (in green) shows

increased intracellular $[Ca^{2+}]_i$ in DMD versus CTR CMs-d-iPSCs, as indicated by the histogram obtained by calculating the intensity of pixels. Scale bar=100μm (**A**). As expected, expression of full-length dystrophin (427 kDa) was absent in DMD compared to CTR CMs-d-iPSCs (**B**). Histograms reveal that DMD CMs-d-iPSCs release significantly higher amounts of cardiac troponin I (cTnI) (**C**) and TNF-α (**D**) compared to CTR CMs-d-iPSCs. Data are presented as mean ± SEM of n=5/8 (**A, B**) and n=6/7 (**C, D**) independent experiments. Student t-test: ***P* < 0.01 and *****P* < 0.0001 vs CTR CMs.

Figure 6. Expression of IP in CTR and DMD CMs-d-iPSCs and the effect of IP inhibition. Measurement of IP expression in CTR and DMD CMs-d-iPSCs. WB analysis reveals that DMD CMs-d-iPSCs up-regulates the IP subunits PSMB8 and PSMB9; however the expression of PSMB5 is unchanged (**A**). Representative staining of CTR and DMD cardiomyocytes with **t**he green fluorescent calcium indicator Fluo-4 AM (in green). Treatment of CTR/DMD CMs-d-iPSCs for seven days (from day 9 post CM differentiation) reverses the increases in $[Ca^{2+}]_I$ - scale bar=100μm - (**B**) and reduces the release of cTnI, meaning that the effect of IP inhibition on lowering cTnI levels is significantly greater for DMD CMs compared to CTR CMs (**C**). RT-qPCR experiments confirm the down-regulation of collagen-3a and TGF-β in treated DMD CMs-d-iPSCs (**D**). Data are presented as mean ± SEM of n=4 to 17 (**A**); n=9 to 11 (**B**); n=3 to 18 (**C**); n=8 (**D**) independent experiments. Statistical analysis was performed by Student t-test (**A, D**: **P* < 0.05, ‡*P* < 0.05, ‡‡*P* < 0.01 vs DMD CMs), 1-way (**B:** ††††*P* < 0.0001 vs CTR CMs) and two-way ANOVA (**C:** §§*P* < 0.01, §§§*P* < 0.001).

Table 1. List of primers for RT-qPCR.

Primer name	Primer Sequence
m-TNFα-f	5'-CTACCTTGTTGCCTCCTCTTT-3'
m-TNFα-r	5'-GAGCAGAGGTTCAGTGATGTAG-3'
m-IL1β-f	5'-TCTGATGGGCAACCACTTAC-3'
m-IL1β-r	5'-GTTGACAGCTAGGTTCTGTTCT-3'
m-CCL2-f	5'-TTTCTTAAATGCAAGGTGTGGA-3'
m-CCL2-r	5'-CCTTGGAATCTCAAACACAAAGT-3'
m-ICAM1-f	5'-AGTAGATCAGTGAGGAGGTGAA-3'
m-ICAM1-r	5'-GCATCCTGACCAGTAGAGAAAC-3'
m-RORγt-f	5'-GACTGACAATCAGCAGGGATAA-3'
m-RORγt-r	5'-GGGAAATACAATGAGGTATTGAAAGG-3'
m-col3a-f	5'-GCCTTCTACACCTGCTCCTG-3'
m-col3a-r	5'-GATCCAGGATGTCCAGAGG-3'

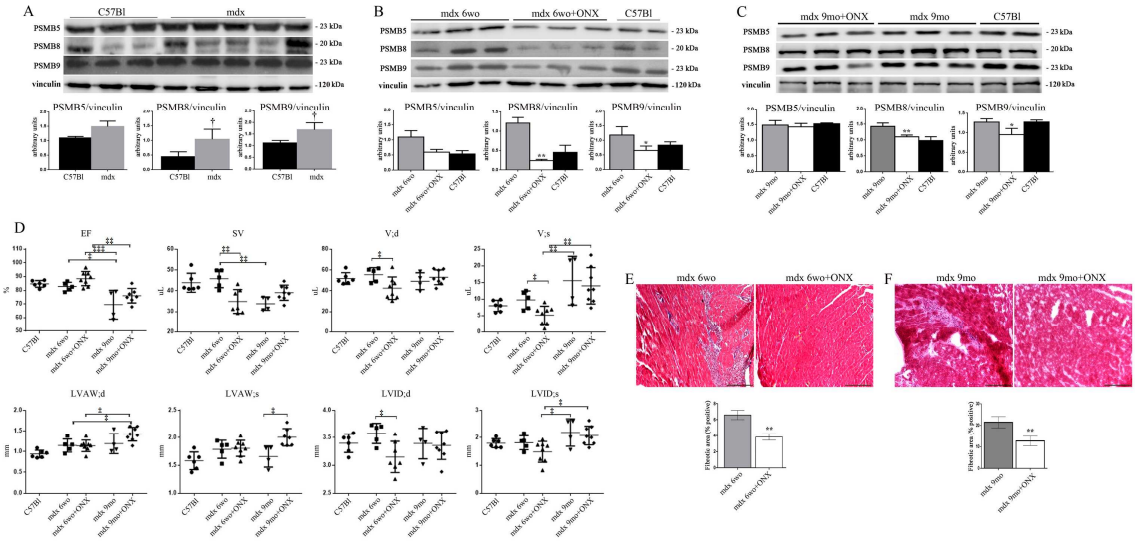

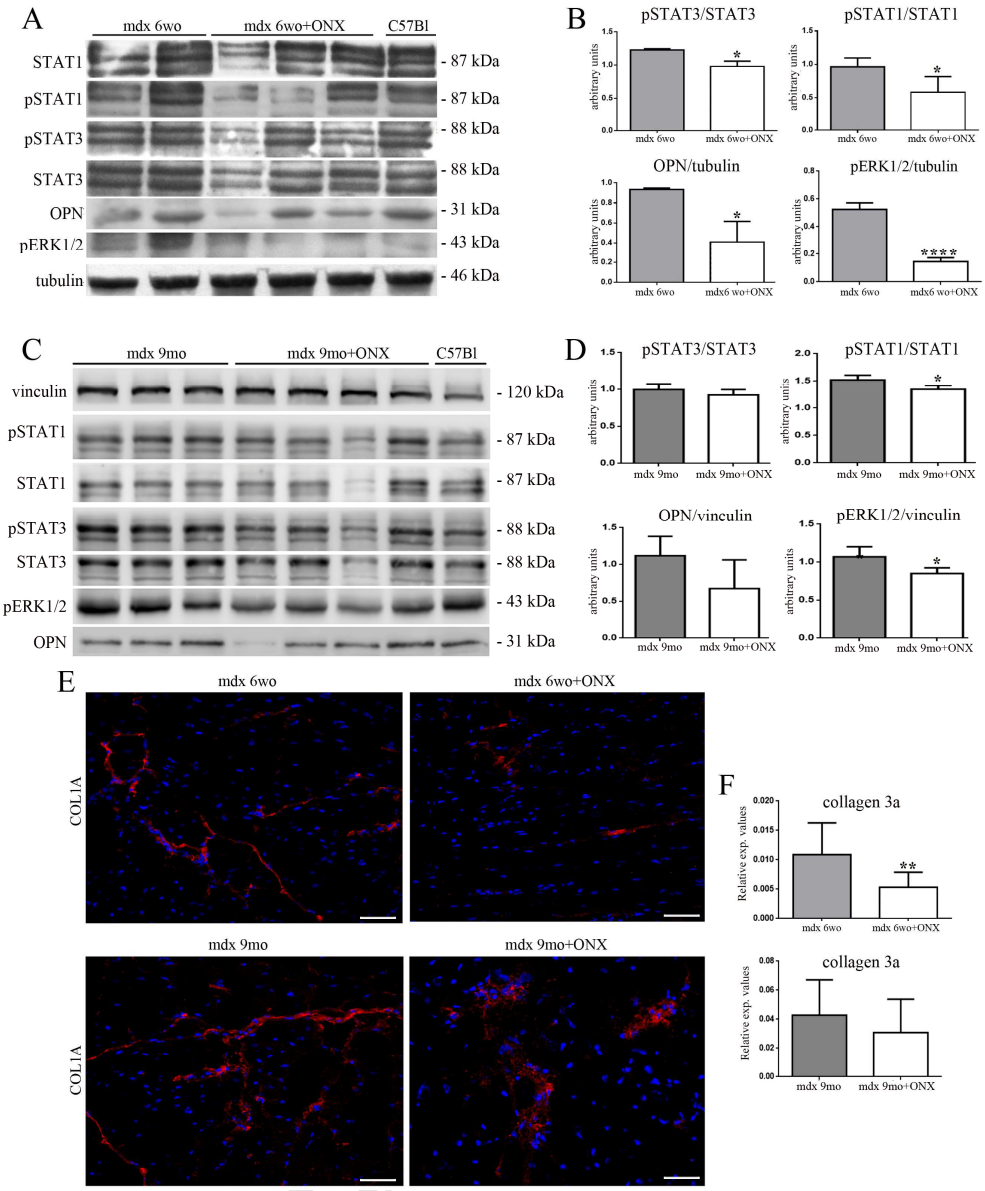
A
mdx 6wo
mdx 6wo+ONX
C57Bl
STAT1
pSTAT1
pSTAT3
STAT3
OPN
pERK1/2
tubulin
- 87 kDa
- 87 kDa
- 88 kDa
- 88 kDa
- 31 kDa
- 43 kDa
- 46 kDa
B
pSTAT3/STAT3
pSTAT1/STAT1
OPN/tubulin
pERK1/2/tubulin
arbitrary units
mdx 6wo
mdx 6wo+ONX
mdx6 wo+ONX
C
mdx 9mo
mdx 9mo+ONX
C57Bl
vinculin
pSTAT1
STAT1
pSTAT3
STAT3
pERK1/2
OPN
- 120 kDa
- 87 kDa
- 87 kDa
- 88 kDa
- 88 kDa
- 43 kDa
- 31 kDa
D
pSTAT3/STAT3
pSTAT1/STAT1
OPN/vinculin
pERK1/2/vinculin
mdx 9mo
mdx 9mo+ONX
E
mdx 6wo
mdx 6wo+ONX
mdx 9mo
mdx 9mo+ONX
COL1A
F
collagen 3a
Relative exp. values
mdx 6wo
mdx 6wo+ONX
collagen 3a
Relative exp. values
mdx 9mo
mdx 9mo+ONX